RSC Advances

PAPER

View Article Online
View Journal | View Issue

Cite this: *RSC Adv.*, 2014, **4**, 62021

# Multi-color cell imaging under identical excitation conditions with salicylideneaniline analogue-based fluorescent nanoparticles†

Hongping Deng,‡[a] Bing Liu,‡[b] Chao Yang,[c] Guolin Li,*[b] Yuanyuan Zhuang,[a] Bo Li*[c] and Xinyuan Zhu*[a]

Six salicylideneaniline (SA) derivatives are synthesized through a condensation reaction. Benefiting from their coplanar molecular conformation and intramolecular hydrogen bonds, three of the compounds are found to exhibit aggregation-induced emission (AIE) or aggregation-induced emission enhancement (AIEE) behavior after self-assembling into nanoparticles that have a diameter of about 50 nm. Based on the excited-state intramolecular proton transfer (ESIPT) properties, these fluorescent nanoparticles (FNPs) display green, yellow or orange colors due to the formation of H- or J-aggregates. Interestingly, FNPs derived from BMSpP show green to green-yellow fluorescence because of the partial transformation of H-aggregates to J-aggregates. Under neutral conditions (pH = 7.4), these FNPs are stable, with the fluorescence intensity decreasing by less than 20% after 120 min, compared to a rapid reduction at pH 5.5. Importantly, a two-photon fluorescence property of FNPs originating from salicylideneaniline or its derivatives is reported for the first time. The two-photon absorption cross-sections of the green, yellow and orange FNPs are found to be 7, 38 and 27 GM, respectively. After conjugation with phospholipids, these FNPs show good water solubility and low cytotoxicity, which make them potential candidates for cell imaging applications. Finally, multi-color cell imaging under identical excitation conditions with single-emissive and multi-emissive FNPs has been achieved. These results are significant for the control of the one- or two-photon fluorescent properties of such derivatives, and provide a promising platform for multi-color cell imaging applications.

Received 8th September 2014
Accepted 10th November 2014

DOI: 10.1039/c4ra10021b

www.rsc.org/advances

## Introduction

In recent years, fluorescent nanoparticles (FNPs) have drawn a great deal of attention for biomedical applications, such as cell-specific targeting,[1] bioanalysis,[2] and detection and identification of proteins.[3] However, FNPs derived from fluorescent tagging methods often suffer from some drawbacks.[4,5] Self-luminescent quantum dots (QDs) are widely applied to imaging and drug delivery because of their long-term stability and the possibility of simultaneous detection of multiple signals.[6] Although QDs are highly fluorescent and photostable, their intrinsic cytotoxicity limits their further bioapplications.[5,7] On the other hand, organic dyes are potential candidates for fabricating FNPs due to their excellent optical properties and low toxicity.[8] Unfortunately, the aggregation of many organic dyes greatly quenches their light emissions based on the aggregation-caused quenching (ACQ) effect, which prevents the development of emissive nanoparticles.[9] In 2001, Tang and his coworkers revealed a type of highly emissive molecule in the aggregated state and defined this phenomenon as aggregation-induced emission (AIE), providing an example for obtaining highly emissive FNPs with organic molecules.[10] Since then, multi-color AIE fluorophores have been developed and widely used in biosensors and cell imaging applications.[11,12] They also proposed the mechanism of the AIE effect to be a process named restriction of intramolecular rotations (RIR) and revealed that the *E–Z* isomerisation was not involved in this process.[13] However, the synthesis of AIE fluorophores with large Stokes shifts in a convenient way is still a great challenge. An efficient method to achieve large Stokes shifts relies on excited-state intramolecular proton transfer (ESIPT) molecules, which have been reported as near infrared (NIR) or multi-color fluorophores, sensors and white luminescence materials.[14–16]

One of the best-known molecules demonstrating the ESIPT phenomenon is salicylideneaniline (SA), which is the most

[a]*School of Chemistry and Chemical Engineering, State Key Laboratory of Metal Matrix Composites, Shanghai Jiao Tong University, 800 Dongchuan Road, Shanghai 200240, P. R. China. E-mail: xyzhu@sjtu.edu.cn; Fax: +86-21-54741297; Tel: +86-21-34203400*

[b]*Department of Oral and Maxillofacial Surgery, The First Affiliated Hospital of Harbin Medical University, 23 Youzheng Street, Nangang District, Harbin 150001, P. R. China. E-mail: liguolin@126.com; Fax: +86-21-54741297; Tel: +86-21-34203400*

[c]*Key Laboratory of Polar Materials and Devices, Ministry of Education, East China Normal University, Shanghai 200241, P. R. China. E-mail: bli@ee.ecnu.edu.cn; Fax: +86-21-54741297; Tel: +86-21-34203400*

† Electronic Supplementary Information (ESI) available: $^{13}$C NMR spectra, TEM data, MTT assays and other characterizations. See DOI: 10.1039/c4ra10021b

‡ These authors contributed equally to this work.

widely studied photochromic and thermochromic Schiff base.[17–19] Also, many derivatives of SA have been synthesized in order to study their spectroscopic and photophysical properties. In 2003, Grabowska and coworkers provided the pico- and femtosecond kinetics of *N*,*N*′-bis(salicylidene)-*p*-phenylenediamine (BSP), which is a famous symmetric derivative of SA.[20] Usually, SA and BSP show very dim fluorescence in solution and little research has focused on their AIE or AIEE properties. In 2004, Yang and coworkers reported the fluorescence enhancement of *N*,*N*′-bis(salicylidene)-*p*-phenylenediamine (BSP) in nanoparticles compared to that in solution and also proposed a mechanism for the enhanced emission.[21] Very recently, Ouyang and coworkers controlled the color and morphology of four electron-donor-substituted AIE compounds.[22] However, these self-assembled structures are generally very large and lack water solubility and stability, precluding cell imaging applications. Previously, we developed a macromolecular nanoparticle approach to obtain FNPs based on RIR of the fluorophore.[23,24] Therefore, we believe that it will be very convenient to fabricate multi-color FNPs with SA derivatives based on RIR and ESIPT.

In the present work, multi-color FNPs are prepared and applied to multi-color cell imaging using SA derivatives. In detail, six SA analogues are easily synthesized through condensation reactions between amino and aldehyde groups. Three of them show bright fluorescence after self-assembly into H- or J-aggregates, owing to their coplanar molecular conformation and intramolecular hydrogen bonds. The morphology of these aggregates is spherical with a diameter of about 50 nm, confirmed by transmission electron microscopy (TEM). Moreover, all the FNPs have good photostability under neutral conditions and pH-responsive properties in acidic environments. Importantly, the two-photon fluorescence of these SA-derived FNPs is proven for the first time. To obtain low cytotoxicity and good water solubility, phospholipids are used to encapsulate these FNPs. Finally, multi-color cell imaging under identical excitation conditions is achieved using single-emissive and multi-emissive FNPs.

# Experimental section

## Materials

*p*-Phenylenediamine, *m*-phenylenediamine, *o*-phenylenediamine, 4-hydroxy benzaldehyde, 3,5-di-*tert*-butyl-2-hydroxybenzaldehyde, salicylaldehyde and 2-hydroxy-4-methoxybenzaldehyde were purchased from Aladdin and 1,2-dioleoyl-*sn*-glycero-3-phosphocholine (DOPC) was purchased from Sigma Aldrich. Ethanol (EtOH) was heated at reflux with calcium oxide and then distilled prior to use. Other reagents and solvents were purchased from Shanghai Sinopharm reagent Co. Ltd., Shanghai, and used without further purification unless otherwise mentioned.

## Characterization

**Nuclear magnetic resonance (NMR).** $^{1}H$ and $^{13}C$ NMR spectra were measured using a Varian MERCURY plus 400 NMR spectrometer at 298 K with deuterated chloroform ($CDCl_3$) or dimethyl sulfoxide-$d_6$ (DMSO-$d_6$) as the solvent. The chemical shifts were referenced to residual peaks of deuterated solvents: $CDCl_3$ (7.26 ppm), DMSO-$d_6$ (2.48 ppm).

**Fourier transform infrared (FTIR) spectroscopy.** FTIR spectra were measured between 4000 and 450 $cm^{-1}$ using a Perkin Elmer Paragon 1000 spectrophotometer. All sample pellets were prepared by grinding the solid sample with dry potassium bromide (KBr) under high pressure.

**High resolution mass spectrometry (HRMS).** HRMS was performed on a Waters Micromass Q-TOF Premier Mass Spectrometer. HRMS data were acquired for each sample from 50 to 1000 Da with a 0.10 s scan time and a 0.01 s interscan delay over a 10 min analysis time.

**Ultraviolet-visible (UV-vis) absorption spectra.** The UV-vis absorption spectra of sample solutions were measured at room temperature in the range of 265–550 nm on a Perkin Elmer Lambda 20 UV-vis spectrometer.

**Fluorescence and quantum yield measurements.** The fluorescence emission measurements were carried out on a PTI-QM/TM/IM steady-state & time-resolved fluorescence spectrofluorometer (USA/CAN Photon Technology International Int.). The excitation wavelength was $\lambda_{ex} = 400$ nm. Fluorescence quantum yields were determined using Rhodamine 6G as the standard ($\lambda_{ex} = 488$ nm, $\Phi = 0.95$). Quantum yields were calculated using the same equation and method as given in the literature.[25]

**Two-photon fluorescence spectra.** The two-photon fluorescence was excited with fs pulses of different intensities at 800 nm using a spectrophotometer (iHR550, HORIBA). The two-photon absorption cross sections were measured with Rhodamine B as the standard.

**Transmission electron microscopy (TEM).** TEM images were obtained using a JEOL JEM-100CX-II instrument at a voltage of 200 kV. Samples were prepared by drop-casting nano-aggregate solutions onto carbon-coated copper grids and then freeze-drying under vacuum before measurements.

## Sample preparation

**Preparation of nano-aggregates.** After all the compounds were dissolved in *N*,*N*′-dimethylformamide (DMF), deionized water was added to the DMF solution *via* a syringe or washing bottle to form a mixed system. Finally, the mixtures were vibrated using an oscillator or just by hand. Then, the mixtures were dialyzed using a dialysis bag (MWCO = 3500 Da) for 12 h before measurements, if necessary. For pH stability and photostability experiments, the mixture was dialyzed against PBS solution (pH = 7.4) and then dilute hydrochloric acid (HCl) was added to tune the pH to 5.5 when necessary.

**Fabrication of single-emissive aggregates.** Due to its excellent biocompatibility and water solubility,[26] DOPC was chosen to encapsulate the different nano-aggregates. Firstly, DOPC was dissolved in a methanol–chloroform (v/v = 1 : 1) mixture and the solvents were removed under reduced pressure to form a thin film. Then, one type of single nano-aggregate solution was added and kept under ultrasound for 20 min.

**Fabrication of multi-emissive aggregates.** Briefly, DOPC was dissolved in a methanol–chloroform (v/v = 1 : 1) solvent

 

mixture to form a thin film after removal of solvents. Then, three types of single aggregate solution were added in a ratio of 3 : 5 : 12 (v/v/v) for **4**, **5** and **6**, respectively. After 20 min sonication, the sample was successfully prepared.

### Cell culture and internalization

L929, A549 or MCF-7 cells were seeded in flexiPERM reusable cell culture chambers in combination with glass coverslips and cultured in DMEM (Dulbecco's modified Eagle's medium) (F-12K was used for A549 cells) supplied with 10% FBS (fetal bovine serum) and antibiotics (50 units per mL penicillin and 50 units per mL streptomycin) at 37 °C under a humidified atmosphere containing 5% $CO_2$. After 24 h of culture, the phospholipid-loaded single- or multi-emissive aggregates were added to the culture wells, and the cells were incubated at 37 °C for 15 min or 30 min. After washing with PBS 3 times, the cells were fixed with 4% formaldehyde for 15 min at room temperature, and then the slides were mounted and observed using a DMI6000B. The excitation wavelength for all samples was 405 nm.

### Cytotoxicity measurements of nano-aggregates

The cytotoxicity of the single-emissive aggregates was estimated using an MTT viability assay against L929 cells. Firstly, L929 cells were placed into 96-well plates at a density of $1 \times 10^4$ cells per well in 200 μL medium. After 24 h, the culture medium was replaced with 200 μL of serial dilutions of aggregate. The cells were cultured for another 48 h. Then, 20 μL of 5 mg $mL^{-1}$ MTT assay stock solution in PBS was added to each well. After 4 h, the medium was carefully replaced with 200 μL of DMSO and the absorbance was measured using a BioTek® Synergy H4 at a wavelength of 490 nm.

## Results and discussion

SA derivatives were facilely prepared using the synthetic route in Scheme 1. By changing the molecular structures of the different reagents, six compounds were synthesized through a conventional condensation of phenylenediamine and phenylenealdehyde with good yields (>95%).[21,22] Details of synthetic procedures and identification are shown in the ESI.† SA derivatives generally form six-membered-ring intramolecular hydrogen bonds between the –OH groups and the N atoms, which can be confirmed from the $^1$H NMR spectra (Fig. 1A).[14] Compound BHPpP (**1**) exhibits a phenol signal at 10.10 ppm due to its incapacity to form intramolecular hydrogen bonds. Compared to BHPpP, the other compounds show significantly downfield phenol signals from 12.93 ppm to 13.93 ppm, giving an obvious indication of the formation of strong hydrogen bonds. It is clear that stronger electron donating abilities result in a greater downfield shift in the phenol signals. Their structure was further characterized by FTIR and $^{13}$C NMR (Fig. 1B and S1†).

To explore the potential optical properties of the six compounds, UV absorbance spectra were measured and are shown in Fig. 2A. Compound BHPpP (**1**) has two absorption

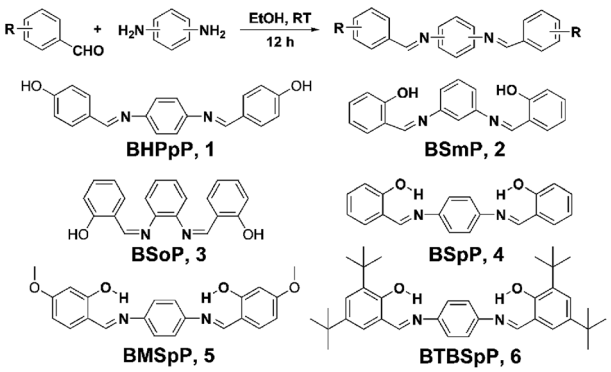


Scheme 1 The synthetic route and chemical structures of SA derivatives *N,N′*-bis(4-hydroxyphenylene)-*p*-phenylenediamine (BHPpP) (**1**), *N,N′*-bis(salicylidene)-*m*-phenylenediamine (BSmP) (**2**), *N,N′*-bis(salicylidene)-*o*-phenylenediamine (BSoP) (**3**), *N,N′*-bis(salicylidene)-*p*-phenylenediamine (BSpP) (**4**), *N,N′*-bis(4-methoxy-salicylidene)-*p*-phenylenediamine (BMSpP) (**5**) and *N,N′*-bis(3,5-bis(tertiarybutyl)-salicylidene)-*p*-phenylenediamine (BTBSpP) (**6**).

bands at about 293 nm and 361 nm, ascribed to the electron transitions of π–π* and n–π*, respectively. Compared to BHPpP, the n–π* transition absorption of BSpP (**4**) red-shifts to 371 nm, while that of the π–π* blue-shifts to 276 nm, which can be attributed to the six-membered-ring intramolecular hydrogen bonds. However, the n–π* transition absorptions of compounds BSmP (**2**) and BSoP (**3**) present a blue-shift phenomenon with the formation of intramolecular hydrogen bonds, which is ascribed to the destruction of the coplanar conformation of the molecules. As a matter of course, the increased electron donating abilities of BMSpP (**5**) and BTBSpP (**6**) result in red-shifts in both the π–π* and n–π* absorptions. Surprisingly, the DMF solutions of all the compounds show very weak or even undetectable fluorescence at room temperature. Considering that SA compounds demonstrate AIE or AIEE characteristics,[21,22] we believe that these SA analogues also have great potential as AIE or AIEE fluorophores by RIR.

The AIE or AIEE characteristics of compounds **1–3** were investigated in DMF–$H_2O$ solutions. Fig. 2B presents the UV absorbance spectra of BHPpP in different DMF–$H_2O$ mixtures. BHPpP has two absorption peaks in pure DMF as mentioned above. However, the second absorption peak, which belongs to the n–π* transition, gradually disappears with the increase in water content, strongly indicating the breakage of the C=N bonds. Indeed, the UV absorption spectrum of BHPpP in DMF–$H_2O$ (1 : 99) is the same as that of the reaction starting materials. The lack of six-membered-ring intramolecular hydrogen bonds leads to the fast breakage of the C=N bonds in BHPpP. For compounds BSmP and BSoP, the destruction of the coplanar conformation results in the heterogeneous formation of J- or H-aggregates, which can be confirmed by the UV absorbance spectra having both red- and blue-shift characteristics (Fig. 2C and D).[27–29] Thus, the nano-aggregates of both BSmP and BSoP show undetectable fluorescence in all DMF–$H_2O$ solutions. In principle, compounds **1–3** act as references to emphasize the importance of intramolecular hydrogen bonds

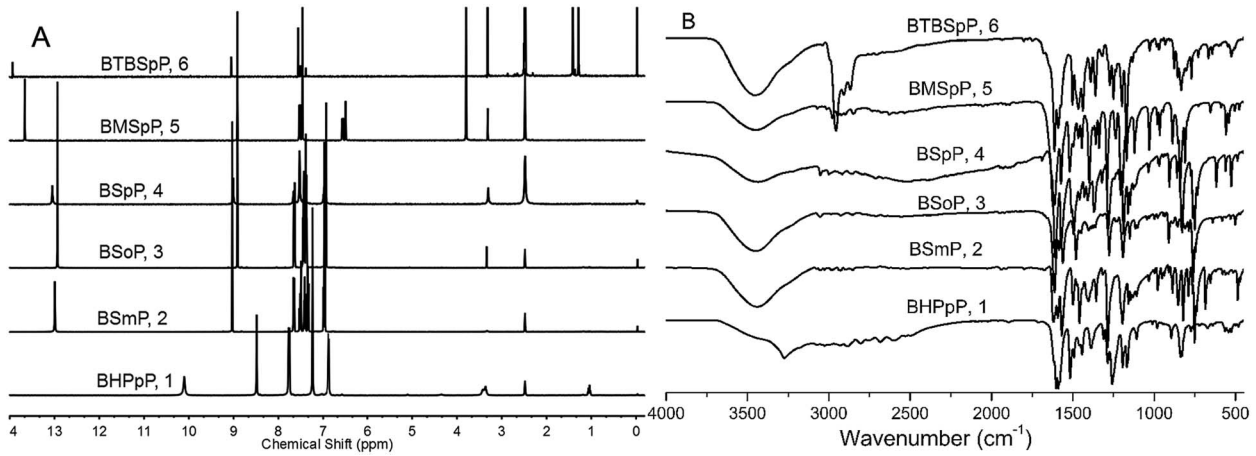


Fig. 1 $^{1}$H NMR (A) and FTIR spectra (B) of salicylideneaniline derivatives BHPpP (**1**), BSmP (**2**), BSoP (**3**), BSpP (**4**), BMSpP (**5**) and BTBSpP (**6**).

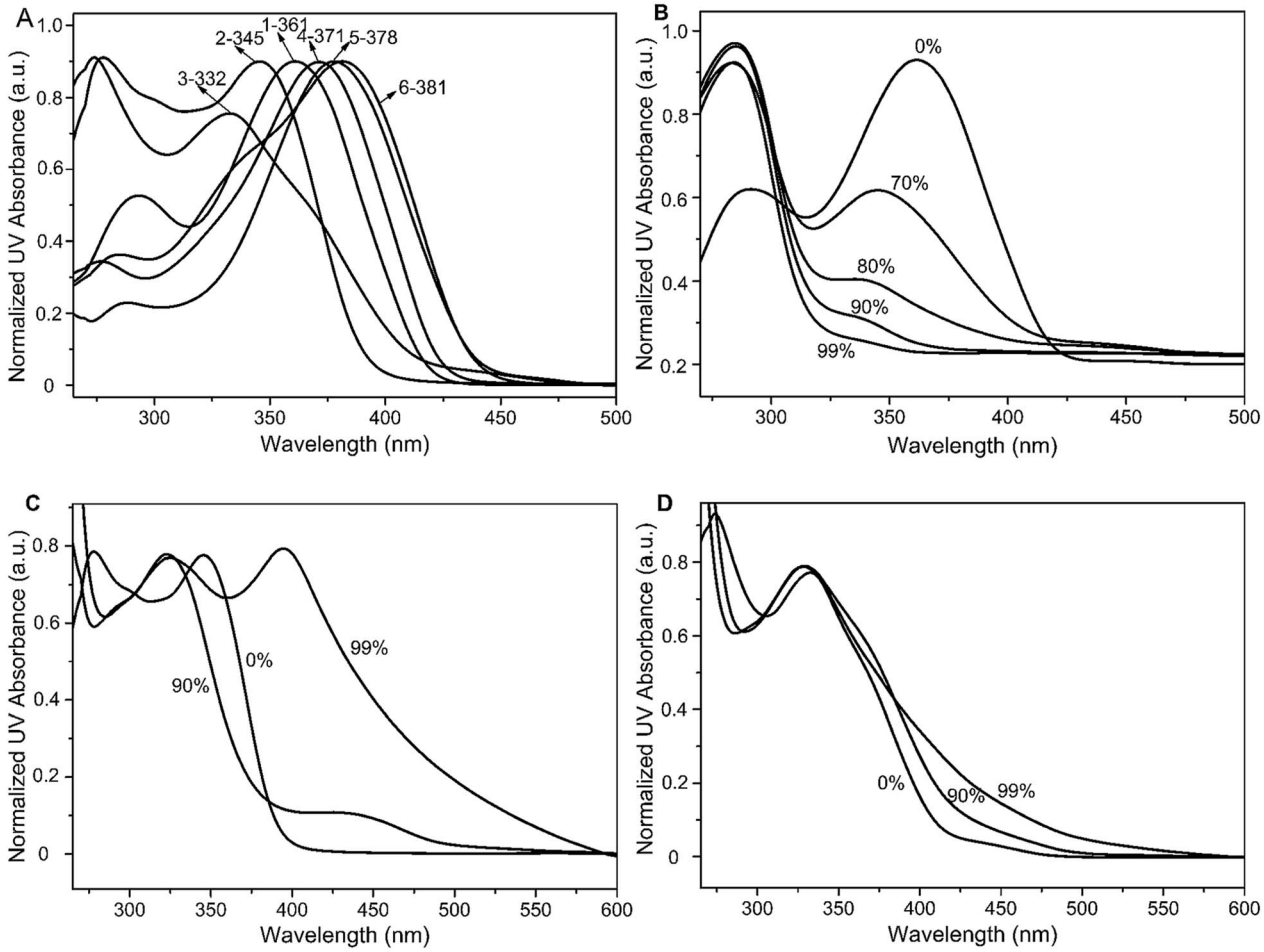


Fig. 2 UV spectra of salicylideneaniline derivatives: (A) BHPpP (**1**), BSmP (**2**), BSoP (**3**), BSpP (**4**), BMSpP (**5**) and BTBSpP (**6**) in DMF; (B) BHPpP (**1**) in DMF–$H_2O$ mixtures; (C) BSmP (**2**) in DMF–$H_2O$ mixtures; (D) BSoP (**3**) in DMF–$H_2O$ mixtures. Water contents (%) are listed.

and coplanar molecular conformation on the AIE or AIEE properties.

In addition, the AIE or AIEE characteristics of compounds **4**–**6** were investigated in detail. BSpP was an accidental discovery that shows an obvious AIE yellow fluorescence after self-assembling into nano-aggregates. Under lower water content (<75%), the UV peak displays both blue- and red-shift potential compared to that with DMF, which can be regarded as a non-

 

equilibrium state. However, a clearly red-shifted UV peak (by about 70 nm) under higher water content indicates the formation of J-aggregates, which is more optimum under 90% water content with a better buffer capacity compared to that with 99% water (Fig. 3A). Moreover, BSpP has undetectable fluorescence in DMF at room temperature. When water (a poor solvent for BSpP) is added to the DMF solution, the emission intensity grows drastically with increasing water content, displaying a clear AIE active feature (Fig. 3B).[10–12] The emission peak is at 547 nm, displaying a large Stokes shift (147 nm) owing to the ESIPT effect.[14,16] With 99% water content, the emission intensity decreases due to the formation of less ordered J-aggregates. Based on these results, BMSpP and BTBSpP were designed and prepared using different salicylaldehyde substituents and their optical properties were also investigated. Compared to BSpP in mixed DMF–$H_2O$ solvents, the UV absorption peak of BMSpP blue-shifts by about 55 nm with an increase in water content (Fig. 3C), which gives a clear confirmation of the formation of H-aggregates.[29] Moreover, the DMF solution of BMSpP shows weak green fluorescence with an emission peak at about 511 nm. With an increase in water content to 90%, the fluorescence intensity increases greatly and the emission peak displays a 6 nm red-shift, while with 99% water content, the fluorescence intensity decreases drastically and the emission peak shows a further 4 nm red-shift (Fig. 3D). These experimental results indicate that BMSpP has an AIEE character and higher (99%) water content is not preferable for the formation of ordered H-aggregates. It is amazing that the nano-aggregates of BMSpP show a green-yellow fluorescence with an emission peak at about 525 nm when adding water at a much faster rate (Fig. S2†). However, the green-yellow fluorescence rapidly vanishes within hours, indicating the formation of unstable aggregates. The UV absorption spectra of BTBSpP in DMF and under low water content (below 80%) are almost identical and

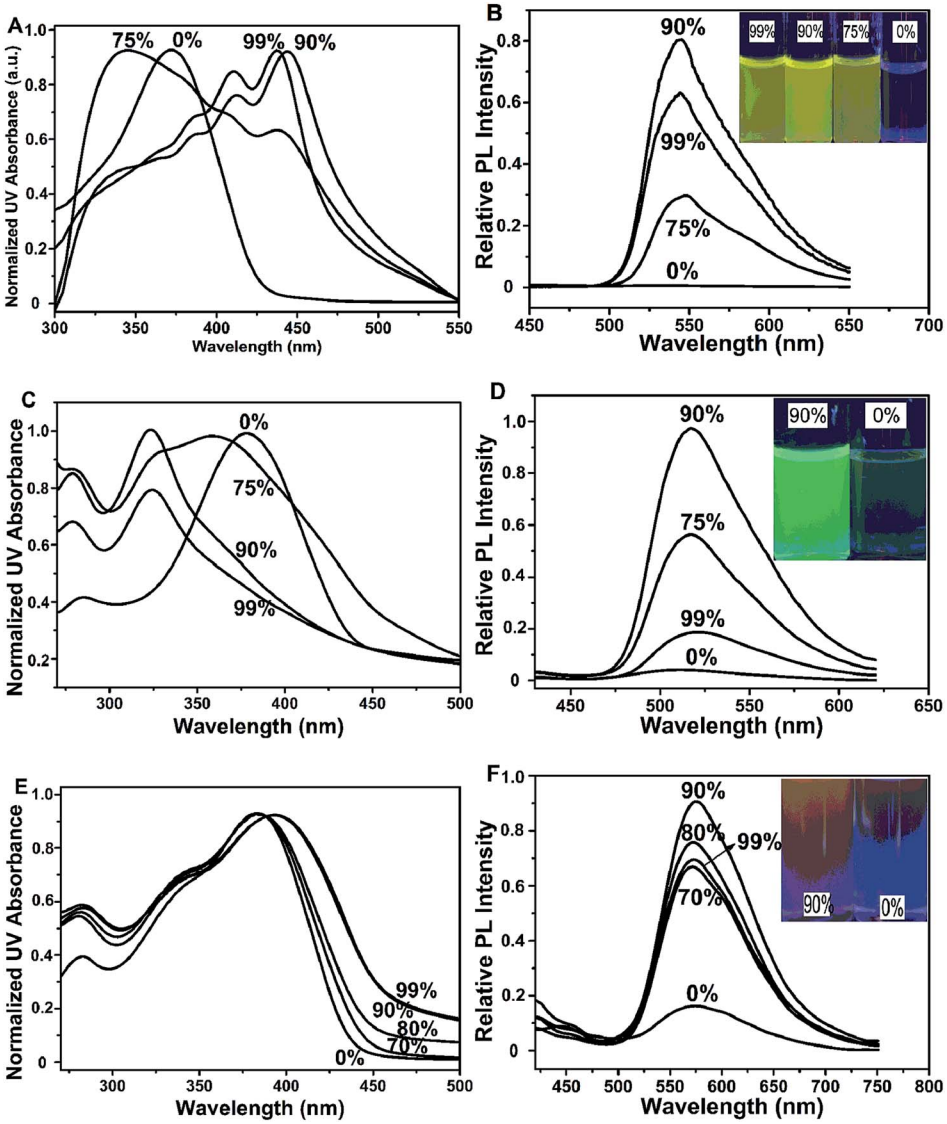


Fig. 3 Normalized UV absorbance and fluorescence emission spectra of SA derivatives BSpP (**4**), BMSpP (**5**) and BTBSpP (**6**) in DMF–$H_2O$ mixtures (10 μM, $\lambda_{ex}$ = 400 nm) with varying volumetric fractions of water: BSpP (A and B), BMSpP (C and D), and BTBSpP (E and F).

only show a red-shift of about 10 nm with high water content (above 90%), demonstrating the formation of weak J-aggregates due to the steric hindrance from the *tert*-butyl groups (Fig. 3E). The fluorescence emission spectrum of BTBSpP in DMF shows a clear emission peak at about 574 nm and the emission intensity increases with increasing water content, which confirms the AIEE feature.[10–12] Just as with BSpP and BMSpP, the emission intensity of BTBSpP decreases under the highest water content , but without an obvious emission peak shift (Fig. 3F). To illustrate the generality of the AIE or AIEE properties of compounds **4–6**, the fluorescence enhancement features for the corresponding FNPs in THF–$H_2O$ and DMSO–$H_2O$ mixtures were also measured and are shown in Fig. S4.† From the results, the fluorescence enhancement behavior is obvious in all the mixed solvents. Thus, the highest fluorescence quantum yields (QYs) of the green, yellow and orange FNPs were found to be 0.10, 0.26 and 0.02, respectively (Table S1†). Subsequently, transmission electron microscopy (TEM) was applied to illustrate the morphology of the FNPs with the highest QYs (Fig. S3†). All of the aggregates present a spherical structure with diameters of about 57 nm, 52 nm, and 48 nm for BSpP, BMSpP and BTBSpP, respectively. For clarity, the UV-vis, fluorescence and two-photon properties along with sizes of all three FNPs are listed and presented in Table S1.†

To confirm the formation of H- or J-aggregates of these compounds, concentration-dependent UV-vis absorption and steady state fluorescence spectra were measured in different mixed solvents. Fig. S5† gives the corresponding results in a DMF–$H_2O$ solvent mixture. At low concentration, the absorption peak of the BSpP nanoparticles is at about 362 nm. With an increase in concentration, an obvious red-shift in the absorption peak is clearly seen with a Stokes shift of about 68 nm, confirming the formation of J-aggregates. However, the fluorescence can not be seen at low concentration. For the BMSpP nanoparticles, a clear blue-shift in the absorption peak with increasing concentration affirms the formation of H-aggregates. In accord with the absorption, the fluorescence peak also shows a blue-shift of about 3 nm with higher concentration, confirming the formation of H-aggregates. However, the absorption and fluorescence peaks of the BTBSpP nanoparticles also display a weak bathochromic-shift with increasing concentration, which indicates the formation of weak J-aggregates. Finally, concentration-dependent absorption and fluorescence spectra were detected in DMSO–$H_2O$ and THF–$H_2O$ solvent

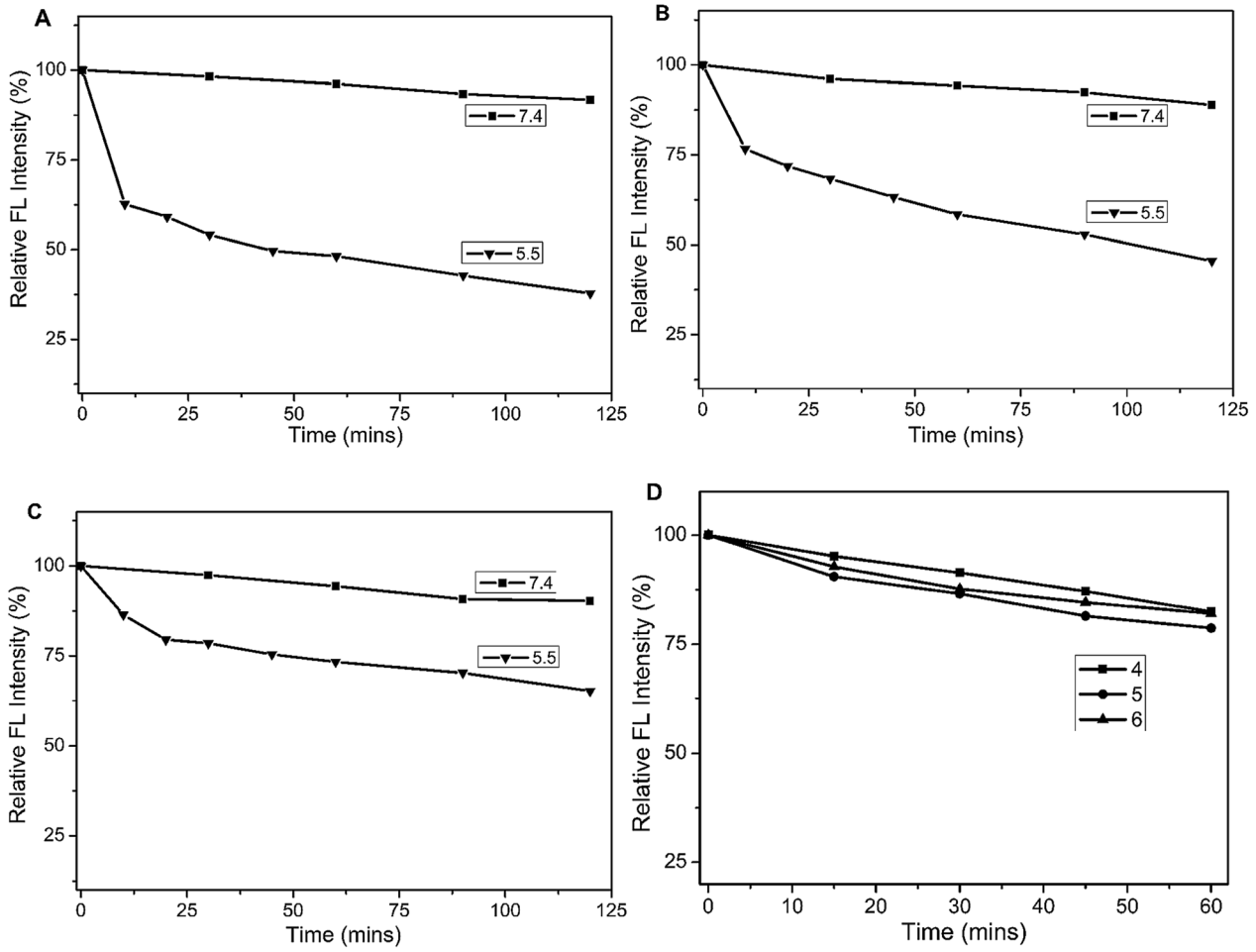


Fig. 4 Fluorescence stability studies under neutral (pH = 7.4) and acidic (pH = 5.5) conditions for BSpP, **4** (A), BMSpP, **5** (B) and BTBSpP, **6** (C), and photostability of nano-aggregates (D, pH = 7.4).

 

mixtures (Fig. S6 and S7†), and almost the same phenomena were observed for these systems, which further illustrates the formation of H- or J-aggregates of these compounds.

Considering that the SA analogues were connected by imine bonds, the pH-responsive properties of the nano-aggregates of different colors were studied in PBS solutions. As shown in Fig. 4, all three nano-aggregates are very stable at pH = 7.4 with the fluorescence intensity decreasing less than 20% after 120 min, in contrast with the rapid degradation of BHPpP (**1**). However, the fluorescence intensity fades rapidly under acidic conditions at pH = 5.5, especially during the first 25 min. However, the rate of fade of the fluorescence intensity decreases

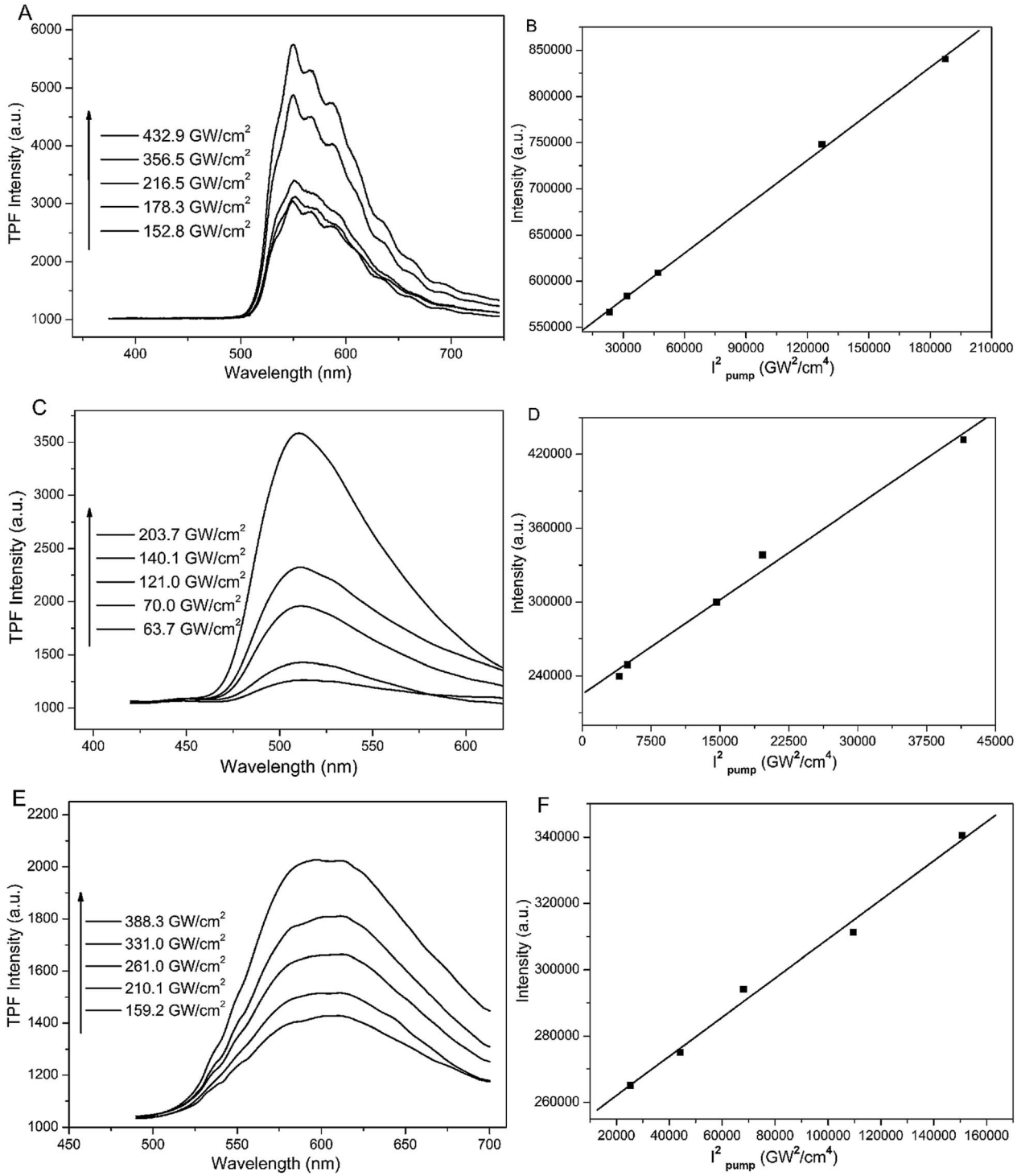


Fig. 5 Two-photon fluorescence emission spectra (A, C and E) and the corresponding linear fitting (B, D and F) of BSpP, BMSpP, and BTBSpP under different excitation powers: BSpP (A and B), BMSpP (C and D), and BTBSpP (E and F).

between BSpP and BTBSpP, indicating the effect of steric hindrance of substituent groups toward the migration of protons. Subsequently, the photostability of the three nano-aggregates in PBS solution at pH = 7.4 was explored and is shown in Fig. 4D. In general, the three nano-aggregates show good photostability with more than 80% fluorescence intensity remaining after 60 min irradiation with a 365 nm lamp.

To our surprise, all three SA-derived FNPs exhibit two-photon fluorescence properties, which have never been reported for SA and its derivatives. In Fig. 5, the two-photon emission spectra recorded under different radiation powers are shown. With an increase in radiation power, the emission intensity increases. The good linear correlation between intensity (area) and the square of pump power confirms the two-photon emission properties of the three FNPs. In addition, the two-photon absorption cross-sections are found to be 38, 7 and 27 GM for BSpP, BMSpP, and BTBSpP nanoparticles, respectively.

To benefit from their bright and multi-colored fluorescence, we intended to use the three types of SA FNP for cell imaging. However, all three FNPs were unstable and aggregated in the cell culture medium, which inhibited their cell applications. To solve this problem, commercial phospholipids were employed to regulate the cell entry of the nanoparticles, due to their good biocompatibility and water solubility.[26] As shown in Fig. S8,† the phospholipid-encapsulated FNPs present little cytotoxicity towards L929 cells even at the highest concentration (10 μM). Subsequently, A549 and MCF-7 cells were cultured with single-emissive nanoparticles and bright fluorescence could be observed after 15 min or 30 min (Fig. S9†). The fluorescence is mostly in the cytoplasm of both types of cell. Subsequently, multi-emissive nanoparticles were prepared by mixing the green, yellow and orange FNPs, and these were then encapsulated with phospholipids. Thus, the multi-emissive nanoparticles were applied in multi-color cell imaging under the same excitation. As depicted in Fig. 6, green, yellow and red fluorescence is very obvious in A549 and MCF-7 cells after culturing for 15 min and 30 min. Indeed, the fluorescence signals are from multi-emissive nanoparticles with the same excitation conditions, which can raise the analysis reliability and accuracy.[30]

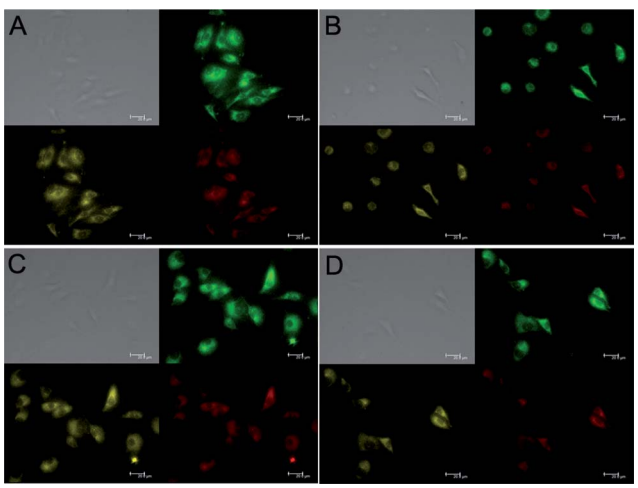


Fig. 6 Multi-color fluorescence imaging of A549 (A and B) and MCF-7 (C and D) cells using multi-emission FNPs for 15 min (A and C) and 30 min (B and D) with green, yellow and red channels under identical excitation conditions. Scale bar = 20 μm. Concentration = 2 μM, $\lambda_{ex}$ = 405 nm.

## Conclusions

In conclusion, six SA derivatives are easily synthesized with high yields using traditional condensation reactions. Due to the ESIPT phenomenon, three chromophores with more coplanar structures show an AIE or AIEE feature after self-assembling into H- or J-aggregates. Moreover, the two-photon fluorescence of the three SA aggregates is confirmed for the first time. Finally, multi-color fluorescence imaging with multi-emissive nano-aggregates is successfully achieved under identical excitation conditions using A549 and MCF-7 cells.

## Acknowledgements

This work was financially supported by the National Basic Research Program (2015CB931801, 2012CB821500, 2013CB834506), and National Natural Science Foundation of China (51473093).

## Notes and references

1 R. Weissleder, K. Kelly, E. Y. Sun, T. Shtatland and L. Josephson, *Nat. Biotechnol.*, 2005, **23**, 1418.
2 R. Gill, M. Zayats and I. Willner, *Angew. Chem., Int. Ed.*, 2008, **47**, 7602.
3 C.-C. You, O. R. Miranda, B. Gider, P. S. Ghosh, I.-B. Kim, B. Erdogan, S. A. Krovi, U. H. F. Bunz and V. M. Rotello, *Nat. Nanotechnol.*, 2007, **2**, 318.
4 C. R. Jing and V. W. Cornish, *Acc. Chem. Res.*, 2011, **44**, 784.
5 X. D. Xue, Y. Y. Zhao, L. L. Dai, X. Zhang, X. H. Hao, C. Q. Zhang, S. D. Huo, J. Liu, C. Liu, A. Kumar, W.-Q. Chen, G. Z. Zou and X.-J. Liang, *Adv. Mater.*, 2014, **26**, 712.
6 I. L. Medints, H. T. Uyeda, E. R. Goldman and H. Mattoussi, *Nat. Mater.*, 2005, **4**, 435.
7 K. T. Yong, W. C. Law, R. Hu, L. Ye, L. W. Liu, M. T. Swihart and P. N. Prasad, *Chem. Soc. Rev.*, 2013, **42**, 1236.
8 L. Yuan, W. Y. Lin, K. B. Zheng, L. W. He and W. M. Huang, *Chem. Soc. Rev.*, 2013, **42**, 622.
9 W. Z. Yuan, P. Lu, S. Chen, J. W. Y. Lam, Z. Wang, Y. Liu, H. S. Kwok, Y. Ma and B. Z. Tang, *Adv. Mater.*, 2010, **22**, 2159.
10 J. Luo, Z. Xie, J. W. Y. Lam, L. Cheng, H. Chen, C. Qiu, H. S. Kwok, X. Zhan, Y. Liu, D. Zhu and B. Z. Tang, *Chem. Commun.*, 2001, 1740.
11 Y. Liu, C. M. Deng, L. Tang, A. J. Qin, R. R. Hu, J. Z. Sun and B. Z. Tang, *J. Am. Chem. Soc.*, 2011, **133**, 660.
12 C. W. T. Leung, Y. N. Hong, S. J. Chen, E. G. Zhao, J. W. Y. Lam and B. T. Tang, *J. Am. Chem. Soc.*, 2013, **135**, 62.
13 N. W. Tseng, J. Z. Liu, J. C. Y. Ng, J. W. Y. Lam, H. H. Y. Sung, I. D. Williams and B. Z. Tang, *Chem. Sci.*, 2012, **3**, 493.

14 K. C. Tang, M. J. Chang, T. Y. Lin, H. A. Pan, T. C. Fang, K. Y. Chen, W. Y. Huang, Y. H. Hsu and P. T. Chou, *J. Am. Chem. Soc.*, 2011, **133**, 17738.
15 D. Maity, V. Kumar and T. Govindaraju, *Org. Lett.*, 2012, **14**, 6008.
16 S. Park, J. E. Kwon and S. Y. Park, *Phys. Chem. Chem. Phys.*, 2012, **14**, 8878.
17 E. Hadjoudis and I. M. Mavridis, *Chem. Soc. Rev.*, 2004, **33**, 579.
18 M. Z. Zgierski and A. Grabowska, *J. Chem. Phys.*, 2000, **112**, 6329.
19 V. Vargas, *J. Phys. Chem. A*, 2004, **108**, 281.
20 M. Zółek, J. Kubicki, A. Maciejewski, R. Naskręcki and A. Grabowska, *Chem. Phys. Lett.*, 2003, **369**, 80.
21 S. Y. Li, L. M. He, F. Xiong, Y. Li and G. Q. Yang, *J. Phys. Chem. B*, 2004, **108**, 10887.
22 C. X. Niu, L. Zhao, T. Fang, X. B. Deng, H. Ma, J. X. Zhang, N. Na, J. S. Han and J. Ouyang, *Langmuir*, 2014, **30**, 2351.
23 H. P. Deng, Q. Zhu, D. L. Wang, C. L. Tu, B. S. Zhu and X. Y. Zhu, *Polym. Chem.*, 2012, **3**, 1975.
24 Y. J. Zheng, G. L. Li, H. P. Deng, Y. Su, J. H. Liu and X. Y. Zhu, *Polym. Chem.*, 2014, **5**, 2521.
25 A. Baldridge, S. H. Feng, Y.-T. Chang and L. M. Tolbert, *ACS Comb. Sci.*, 2011, **13**, 214.
26 K. Raemdonck, K. Braechmans, J. Demeester and S. C. D. Smedt, *Chem. Soc. Rev.*, 2014, **43**, 444.
27 T. E. Kaiser, V. Stepanenko and F. Würthner, *J. Am. Chem. Soc.*, 2009, **131**, 6719.
28 F. Würthner, T. E. Kaiser and C. R. Saha-Möller, *Angew. Chem., Int. Ed.*, 2011, **50**, 3376.
29 R. J. Dong, B. S. Zhu, Y. F. Zhou, D. Y. Yan and X. Y. Zhu, *Angew. Chem., Int. Ed.*, 2012, **51**, 11633.
30 F. C. Alexandra, M. S. Chad, N. Iuliia, P. Stéphane and V. E. Svetlana, *Angew. Chem., Int. Ed.*, 2014, **53**, 2927.